www.elsevier.com/locate/csr

Tide model comparison over the Southwestern Atlantic Shelf

Martin Saraceno, E.E. D'Onofrio, M.E. Fiore, W.H. Grismeyer

PII: S0278-4343(10)00271-2
DOI: doi:10.1016/j.csr.2010.08.014
Reference: CSR 2247

To appear in: *Continental Shelf Research*

Received date: 25 January 2010
Revised date: 19 August 2010
Accepted date: 31 August 2010

Cite this article as: Martin Saraceno, E.E. D'Onofrio, M.E. Fiore and W.H. Grismeyer, Tide model comparison over the Southwestern Atlantic Shelf, *Continental Shelf Research*, doi:10.1016/j.csr.2010.08.014

TIDE MODEL COMPARISON OVER THE SOUTHWESTERN ATLANTIC SHELF

Martin Saraceno (1,2), E.E. D'Onofrio (2,3,4), M.E. Fiore (2,3), W.H. Grismeyer (3).

(1): Centro de Investigaciones del Mar y la Atmósfera (CIMA), Intendente Guiraldes 2160, Ciudad Universitaria, Pab. II, 2do piso, Ciudad de Buenos Aires, C1428EGA, Argentina. Email: saraceno@cima.fcen.uba.ar

(2) Departamento de la Atmósfera y los Océanos, FCEyN, Universidad de Buenos Aires,

Intendente Guiraldes 2160, Ciudad Universitaria, Pab. II, 2do piso, Ciudad de Buenos Aires, C1428EGA, Argentina.

(3) Departamento de Oceanografía, Servicio de Hidrografía Naval, Av. Montes de Oca 2124, Ciudad de Buenos Aires, C1270ABV, Argentina.

(4) Instituto de Geodesia y Geofísica Aplicadas, Facultad de Ingenieria, Universidad de Buenos Aires, Av. Las Heras 2214, 1127, Ciudad de Buenos Aires, Argentina.

ABSTRACT

Sea Surface Height (SSH) as measured by satellites has become a powerful tool for oceanographic and climate related studies. Whereas in the open ocean good accuracy has been achieved, more energetic dynamics and a number of calibration problems have limited applications over continental shelves and near the coast. Tidal ranges in the Southwestern Atlantic (SWA) continental shelf are among the highest in the world ocean, reaching up to 12 m at specific locations. This fact highlights the relevance of the accuracy of the tidal correction that must be applied to the satellite data to be useful in the region. In this work, amplitudes and phases of tidal constituents are extracted from five global tide models and three regional models and compared to the corresponding harmonics estimated from coastal tide-gauges (TGs) and satellite altimetry data. The Root-Sum-Square (RSS) of the misfit of the common set of the five tidal constituents solved by the models (M_2, N_2, S_2, K_1 and O_1) is higher than 18 cm close to the coast for two of the regional models and higher than 24.5 cm for the rest of the models considered. Both values are too high to provide an accurate estimation of geostrophic non-tidal currents from satellite altimetry in the coastal region. On the other hand, the global model with the highest spatial resolution has a RSS lower than 4.5 cm over the continental shelf even when the non-linear M_4 overtide is considered. Comparison with in-situ current measurements suggests that this model can be used to de-tide altimetry data to compute large-scale patterns of SSH and associated geostrophic velocities. It is suggested that a local tide model with very high resolution that assimilates in-situ and satellite data should meet the precision

needed to estimate geostrophic velocities at a higher resolution both close to the coast and over the Patagonian shelf.

1. INTRODUCTION

1.1 The Southwestern continental shelf circulation and tidal regime

The mean width of the Southwestern continental shelf ranges between 200 km and 800 km. It is narrow in the north and enlarges up to 800 km at 51ºS (Figure 1). Roughly it extends from 30ºS to 55ºS and from the coastline to the 300m isobath, where a pronounced shelf-break clearly divides the continental waters from open waters.

The circulation over the shelf depends on the propagation of tidal waves, wind forcing, freshwater discharges, and the influence of neighboring western boundary currents. The relative contribution of each of these forcings to the circulation patterns varies among regions. According to recent numerical experiments, the shelf circulation is dominated by the equatorward Malvinas current that flows along the shelf-break slope (Palma et al., 2008). Tides and strong offshore winds play an important role as well (Palma et al., 2004). The strong tidal currents increase near-bottom mixing, which reaches the sea surface and generates fronts (Acha et al., 2004). Tide fronts in the Patagonian shelf have been shown to play a major role in CO_2 absorption from the atmosphere (Bianchi et al., 2005). The high turbulent mixing and the local circulation enhance nutrient availability in the euphotic zone inducing high primary productivity (Romero et al., 2006). Farther north, in the Brazilian sector, the circulation is dominated by the poleward flow of the Brazil Current and the freshwater discharges from the Río de la Plata and the Lagoa dos Patos (Piola et al., 2008).

The description of the tidal regime in the SWA shelf is based mostly on the analysis of model efforts. Few in-situ data obtained from current meter and tide gauge measurements exist. Thus knowledge of the region is limited by the latter point and only large scale patterns based on the observation of a qualitatively agreement between the different model outputs can be made. The SWA continental shelf presents a complex pattern of tidal amplitudes and phases. The range of tidal amplitudes decreases from up to 4.5m in the southern end of the Argentinean shelf to a few centimeters in the Brazilian sector (Figure 2; Panella et al., 1991). South of about 42ºS shelf tides reach exceptional amplitude (Glorioso and Flather, 1997). The tidal component that presents the largest amplitude (up to 3.7m) in the whole domain is the lunar semi-diurnal M_2 (Figure 3). M_2

presents two amphidrome systems located approximately at 41ºS and 48ºS (e.g. Palma et al., 2004; Figure 2). The spatial and temporal structures of the S_2 and N_2 harmonics are similar to the M_2 structure although with a substantially smaller amplitude (not shown). A calculation of the amplitude ratio $F = (M_2 + S_2)/(K_1 + O_1)$ indicates that the inner portion of the southern shelf is dominated by semidiurnal tides and that the outer portion and the northern shelf is dominated by mixed tides (Genco et al., 1994; Khanta, 1995; Le Provost et al., 1994; Glorioso and Flather, 1997; Palma et al., 2004).

Based on three current meter measurements located at the same latitude Rivas (1997) reported that the tidal forcing accounts for more than 90% of the kinetic energy variance in the inner portion of the Patagonian Shelf ($z < 50$ m) and at least half of the variance of the outer shelf. Zavialov et al. (2002) analyzed a 6-month current meter record at a mooring site in the South Brazilian Shelf (34ºS to 28.5ºS) and concluded that the diurnal tides are more important than the semidiurnal tides. Castro and Miranda (1998), however, observed that in the South Brazil Bight (28.5ºS to 23ºS) the semidiurnal tides account for more than 50% of cross-shelf current variability.

Thus it is clear that a tidal analysis from a uniform and wide coverage as provided by satellite altimetry will certainly benefit the knowledge of the tidal regime in the region. This has been partially done by global models that assimilate altimetry data. Global models are validated against global data sets of tide gauges and, despite the fact that most of them recognize that important in-homogeneities arise from the Patagonian shelf, none of them validated their results in this specific region. This work tries to fill that gap, by evaluating global as well as regional tidal models.

Accurate tidal modeling is very important in the region since the interaction between tides and large surges may cause significant flooding in high density populated regions (D'Onofrio et al., 1999; Fiore et al., 2009). Furthermore, accurate removal of the tidal component from the satellite altimeter data will allow, for the first time, a large scale study of the circulation over the Southwestern continental shelf based on satellite altimeter observations.

1.2 Tidal modeling in the SWA Ocean

Several efforts have been made to implement local tide models to study the behavior of storm surges and their interaction with tides over the shelf: Glorioso, (2000) developed one of the first 3D tide and surge models. Later, Palma et al., (2004) and Simionato et al., (2004) developed tide

models and Etala, (2009), a tide and storm surge model. The latter three models are considered here and their main characteristics are summarized, along with five global models, in Section 2.

Increased computational capacity and the availability of long and accurate time series of satellite altimetry data have made possible the implementation of high-resolution global tide models, which do not depend on critical boundary conditions. Deep ocean tides have been estimated with unprecedented precision and accuracy by fitting altimetry data to empirical functions derived from numerical hydrodynamic models (Cartwright and Ray, 1990; Desai and Wahr, 1994; Eanes and Bettadpur, 1995; Le Provost et al., 1998). This success has been achieved thanks to: (i) TOPEX design which allowed separating tidal aliases (Parke, 1987), (ii) precise satellite orbit and tracking determination and (iii) advances in modeling and data assimilation. However in marginal seas and near the coast the results are not as good. Coastal processes are more difficult to resolve with altimeter data, due to two types of problems. First, and most importantly, intrinsic difficulties affect the corrections applied to the altimeter data near the coast. Two examples are the wet tropospheric component (very different in coastal regions) and the frequency of oceanographic signals (much higher than in deep waters). Thus, data are usually flagged as unreliable within some distance to the coast. Second, the interpolation of along-track data collected by just one or two satellites provides only marginal resolution of mesoscale and smaller-scale structures in ocean circulation (Chelton and Schlax, 2003; Le Traon and Dibarboure, 2002; Leeuwenburgh and Stammer, 2002), which are dominant in the coastal regions. Therefore, the accuracy of tide models which assimilate satellite altimetry data is lower in marginal seas and close to the coast compared to deep ocean waters (e.g. Andersen et al., 1995).

Several approaches are available to address the problems described above. Pascual et al. (2006, 2007) showed that increasing the number of satellites used to produce gridded maps of SSH to four greatly increases the accuracy of the mesoscale surface circulation estimated. Volkov et al., (2007) showed that improvements in tidal and high frequency models used to produce the data distributed by the AVISO (Archiving Validation and Interpretation of Satellite Data in Oceanography) Project also improve the quality of the altimeter SSH fields over wide continental shelves. However, over the Patagonian shelf, the gridded AVISO SSH data still show problems, as indicated by the disorganized pattern shown in the eddy propagation field (Fu, 2009) and the low correlation obtained with coastal TGs (Saraceno et al., 2008b).

1.3 Objectives

Global gridded maps of SSH are produced using global tide models to de-tide the along-track data. AVISO uses GOT00 (Ray, 1999) and is now moving to GOT4.7 (Ray, 1999). In others regions of the ocean where important tides exist as well, it has been shown that regional models can more accurate by correct the altimeter data than global ones (Burrage et al., 2003; Cherniawsky et al., 2004; Foreman et al., 1998; Matsumoto et al., 2000). The objective of this work is to evaluate which tide model works best in the SWA continental shelf. The evaluation will be carried out through comparison of the tidal constituents obtained by models, tide-gauges and satellite altimetry data. The tide-gauges used are distributed along the Argentinean coast (Figure 1). Satellite altimetry data are analyzed at the crossover locations of the ascending and descending paths over the SWA continental shelf (Figure 1). The five constituent M_2, N_2, S_2, K_1 and O_1 that are the common set provided by the selected models (Table 2) will be considered. From Figure 3, and the description provided above (Section 1.2), it is clear that, apart from M_2 that clearly dominates the tidal regime everywhere in the shelf, the order of importance of the constituents depends on the location considered. In particular, it is worth noting the amplitude of the M_4 overtide, which reflects the importance of the interactions of resonant modes over the shelf (Figure 3, Palma et al., 2004). A discussion on how the results presented in Section 3 change when the constituents Q_1, P_1, K_2 and M_4 are included is provided in Section 4, for those models that do provide these constituents.

1.4 Article outline

The present article is organized as follows: data and the methodology used are presented in Section 2, results are presented in Section 3; final remarks and a discussion conclude the article in Section 4.

2. DATA AND METHODOLOGY

2.1 Tide Gauges

The Naval Hydrographic Service (SHN) of Argentina provided coastal tide gauge (TG) tidal amplitudes and phases used in this work. The same values are routinely used for the official tidal prediction (SHN, 2008). The location of the TGs is indicated in Figure 1. Table 1 provides latitude, longitude, type of device and length in days of the time series analyzed for each TG. Amplitudes

and phases have been estimated through harmonic analysis using the least squares method. Two factors are critical to accurately estimate harmonic tidal constants and avoid aliasing problems: the length and the sampling interval of the time series analyzed. The longest time sampling corresponding to some of the tide pole measurements is 30 minutes which is short enough to establish the tidal constants considered. Thus the length of the time series is the unique factor that may prevent the determination of the tidal constituents considered from a theoretical point of view. In practice, the different TGs have different errors associated with the instrument and/or measurement method used. To stay on the conservative and safe side, we decided to use only the most energetic and dominant tidal constituent M_2 for all the TGs and to include eight of the tidal constituents estimated by the majority of the models considered for only four TGs. The eight tidal constituents included in the analysis are S_2, N_2, O_1, K_1, Q_1, P_1, K_2 and M_4. The four TGs were carefully selected considering the following criteria. Most of the TGs are located inside harbours that in turn are located inside bays or estuaries; thus we first selected those that were more exposed to the open ocean. We also did not consider TGs located inside the mouth of the Río de la Plata since there, tides are affected by the dynamics of river discharge (Simionato et al., 2004) and we wish to focus more on the continental shelf. We then considered the length of the time series, the type of instrument used (Table 1) and possible problems in the measurements that may affect estimation of any of the eight tidal constituents mentioned above. The four TGs selected by this procedure are located at Mar del Plata, Puerto Deseado, Puerto Madryn and Punta Loyola (Figure 1).

2.2 Altimetry data

T/P, J-1 and J-2 satellite periodicity is 9.9156 days. Extracting time series from the crossovers of the ascending and descending passes allows the number of observations to be doubled for a given period of time and helps to significantly decrease the aliasing problem (e.g. Parke, 1987). We selected 84 crossover points over the SWA continental shelf length at less than 300 m water depth. SSH used here was produced by CTOH (Centre de Topographie des Océans et de l'Hydrosphère, http://ctoh.legos.obs-mip.fr/). CTOH reprocessed T/P, J-1 and J-2 data over the SWA continental shelf. This was obtained from the GDR (Geophysical Data Record) data stream provided by AVISO, at a rate of one per second (6-7 km along track spacing), with additional validated corrections aimed to improve the quality of the data over the shelf (Cancet et al., 2009). The sea state bias, loading effect, ocean tide, solid tides, inverse barometer effect, wet troposphere, dry

troposphere and ionosphere corrections terms have been recomputed and/or a different model has been used respect to the standard corrections available with the GDR data (Cancet et al., 2009). Thanks to the reprocessing done, CTOH SSH data show a significant improvement (decrease of the RMS of the SSH) over continental shelf and coastal areas (Cancet et al., 2009). The ocean tide is left as an independent variable in order to allow the user to subtract it from the SSH. CTOH has also blended T/P, J-1 and J-2 missions subtracting the difference among missions. This allows analyzing more than 15 years of data. After downloading the dataset, we extracted the 84 time series at the crossover points (Figure 1) and added the oceanic tidal signal to the SSH at each along-track point provided by CTOH. The time series spanned the period March 1993 to April 2008. Each time series has about 1118 records, which is twice the number of records obtained at a location over a non-crossing point along a track for the time period considered.

2.3 Tide Models

We used four global (FES04, GOT00, GOT4.7, EOT08a), one regional (TPXO_AO) and three local (Simionato, Palma and SMARA) tide models. The regional model covers the whole Atlantic Ocean and the local models only the Southwestern Atlantic. For simplicity, we will refer to the regional model TPXO_AO as a global one, since its domain is by far much larger than the other local ones. The global models selected are among the most popular tide models used and are, to our knowledge, improved versions of tide models that have been continuously evolving during the modern satellite altimetry era. On the other hand, this study does not pretend to realize a complete classification of all the tide models available. GOT00, an older version compared to GOT4.7, is explicitly included here for comparison purposes since these are the models consecutively selected by AVISO to de-tide altimeter data and produce gridded fields. TPXO_AO and the three local models use boundary conditions obtained from global ones. Local models do not assimilate any data inside their domain and they use a customized bathymetry. The five non-local tide models incorporate observed tidal information. The eight models are listed in Table 2 where the type of incorporate data, the spatial resolution and the corresponding citation are indicated. A short description of each model is provided below. The reader interested on further details concerning each model is strongly encouraged to refer to the literature cited in Table 2.

Finite Element Solution tide model called FES2004, an update of FES99, is based on the nonlinear barotropic shallow water equations, with bottom friction parameterized through a quadratic

dependency on local tidal velocities and through tidal forcing derived from astronomical potential and including earth tide, ocean tide loading and shelf attraction. Fifteen tidal constituents are distributed on 1/8° grids and new tide loading effects were also computed. The accuracy was improved by assimilating tide gauge and altimetry data (T/P and ERS-2) through a revised representer assimilation method (Lyard et al., 2006).

Goddard Ocean Tide model GOT99.2 is an empirical solution for the amplitudes and phases of the global oceanic tides, based on over six years of sea-surface height measurements by the T/P satellite altimeter and is an adjustments of FES94.1 on a 0.5 by 0.5 degree grid. GOT4.7 is an update to GOT00 that is in turn an update to GOT99.2 (Ray, 1999).. Ten tidal constituents are distributed on 1/8° grids. GOT4.7 uses empirical co-tidal and co-range mapping to incorporate tidal constant.

EOT08a is an empirical ocean tide model from multi mission satellite altimetry. Ten tidal constituents are distributed on 1/8° grids. A cross calibration was performed by a global crossover analysis based on nearly simultaneous single and dual satellite crossover differences performed between all altimeter systems operating contemporaneously. EOT08a uses empirical co-tidal and co-range mapping to incorporate tidal constant (Savcenko and Bosch, 2008).

TPXO_AO is a regional model that covers the Atlantic Ocean. It is a modification of the TPXO7.1 global inverse tide model developed by Gary Egbert and Lana Erofeeva at Oregon State University (Egbert and Eerofeeva, 2002). There were assimilated 531 cycles of T/P and J1 data; 114 cycles of Topex Tandem data (in shallow water) and 108 cycles of ERS data (in shallow water and above 66°N). Eleven tidal constituents are distributed on 1/12° grids.

Simionato model is a regional application based on the three-dimensional primitive equation model developed at the University of Hamburg (HamSOM) by Backhaus (1983, 1985). Nine tidal constituents are distributed on a 1/3° x 1/4° grid. Thirteen vertical levels have been used. An advantage of using a multi-layer model even when density is constant is to allow for a better representation of the bottom friction. In the HamSOM model, the bottom stress is parameterized by means of a quadratic law in terms of the horizontal velocity vector at the bottom layer of the model and the vertically averaged horizontal velocity in a frictional layer close to the bottom (Simionato et al., 2004).

Palma model is a regional application based on the Princeton Ocean Model (POM). The model equations, and the numerical algorithms used to solve them, have been described in detail by Blumberg and Mellor (1987). The model solves the three-dimensional primitive equations on an

Arakawa C grid. The numerical scheme conserves linear and quadratic quantities like mass and energy. The model domain extends from 55ºS to 20ºS and from 70ºW to 40ºW. Five tidal constituents are distributed on a curvilinear horizontal grid with 250 grid points in the along-shelf direction, with an average resolution of 7.5 km, and 150 grid points in the cross-shelf direction, with an average resolution of 10 km. In the vertical the model equations are discretized in 25 sigma levels with small spacing at the top and the bottom to provide higher resolution of surface and bottom boundary layers.

SMARA is a regional barotropic model which solves the hydrodynamics equations on an Arakawa C grid (Etala, 2010, personal communication). The model domain extends from 54° 30' S to 32° 30 'S and from 51° 10' W till the South American coast. Five tidal constituents are distributed on a 1/3° x 1/3° grid. The model uses the results provided by the Schwiderski global tide model (Schwiderski, 1978, 1980) at the boundaries. Further details can be found in http://www.hidro.gov.ar/SMARA/plataforma6.pdf.

2.4 Methodology

Amplitudes and phases obtained from the TGs and from satellite altimeters at the crossovers of the tracks are compared with corresponding values obtained from the models (Table 2). Since some tide models considered assimilate altimetry data, it may be argued that the harmonics extracted from altimetry data at the crossovers of the ground track data does not represent an independent database for comparison. However, as may be argued from the results obtained, error propagation inherent to each tide model plays an important role, especially in shallow waters. It is thus not redundant to compare harmonic constants extracted from tide models that assimilate data with those extracted directly from the altimetry data. Error propagation may be due to the fact that models are not able to solve adequately the short temporal and spatial tidal scales that exist over the Patagonian shelf, nor to solve adequately amplification of internal tides or dissipation effects which tend to amplify in this region (e.g. Glorioso, 2000). The altimetry time series constructed at the crossover locations have enough data to precisely separate the nine constituents considered in this work (Schrama and Ray, 1994). It is thus possible to estimate the harmonic constants by least squares fitting.

Comparison of the tidal constituents along the coast (i.e. models vs. TGs) is separated from that over the shelf (i.e. models vs. satellite altimetry). To quantify the misfit between each model and the coastal tide gauges the following formula have been used for each tidal constituent:

$$RMS_{misfit} = \left(\frac{1}{N} \sum_{N} \frac{1}{2} \left[[H_1 \cos(g_1) - H_2 \cos(g_2)]^2 + [H_1 \sin(g_1) - H_2 \sin(g_2)]^2 \right] \right)^{1/2} \quad (1)$$

where N is the number of tide gauges used, H_1 and g_1 are respectively the amplitude and Greenwich phase lag obtained from the TGs, and H_2, g_2 are respectively the amplitude and Greenwich phase lag provided by the models. The same formula was used to estimate the misfit between the models and the altimetry satellites measurements at the crossover locations (in this case N is the number of crossover locations).

For each TG and altimetry crossover point we selected the nearest non-land grid point of each model to extract amplitudes and phases using an automated program. We preferred to use this criteria to do the comparison and not to interpolate all the different model grids to a common grid because: (i) we avoid any bias by the interpolation technique used- the coastal and shelf seas are by far the most complicated areas of the ocean to model and even a simple variable as the SSH cannot be easily interpolated; (ii) the objective of this work is to compare each model "as is", i.e. to objectively compare the model's results with the observations without altering them in any way.

3. RESULTS

3.1 Coastal analysis: comparison to TGs

Considering all the TGs (dataset 1), global models get better results than regional ones for the M_2 component, led by EOT08a and FES04 (Figure 4 and Table 3). This result suggests that models performing data assimilation or incorporate empirical mapping of the tidal constituent, have a better agreement with in-situ data compared to the local models analyzed here, which do not assimilate any data. However considering the four selected TGs (dataset 2), the Simionato and Palma local models obtain a better agreement with the TGs for M_2, led by Palma's model (Figure 4 and Table 3). Inspection of the spatial distribution of the RMS misfit for M_2 (not shown) reveals that Palma's model has the largest misfits for stations 13-16, a fact that probably explains the poor result of this model obtained for M_2 when all TGs are considered. A similar argument applies to the Simionato model, i.e. Simionato gets worse results compared to global models with dataset 2 than with dataset 1 because of a large misfit obtained at some stations that are part of dataset 1 and not of dataset 2. SMARA and the five global models considered are in the opposite situation: they get worse results

with dataset 2 than with dataset 1. This is due to the fact that the RMS misfit of dataset 2 presents higher values than the values obtained with the TG stations that are part of dataset 1 but not of dataset 2. In fact, most of those stations are located in the northern part of the shelf (Figure 1), where tidal amplitudes are much lower than in the southern region and therefore RMS misfit are much lower as well.

The lowest Root Sum Square (RSS) obtained from the RMS misfits of the 5 tidal constituents M_2, N_2, S_2, O_1 and K_1 with data set 2 (Figure 5) is obtained by Palma and Simionato (18.2 cm and 19.2 cm respectively) by a large difference (5 cm or more) compared to the rest of the models. RMS misfit values that we obtained are large compared to results obtained globally by other authors. Shum et al. (1997) compared 15 global models with 107 TGs around the world and obtained only 3.9 cm as the highest RMS misfit for M_2. RMS misfit strongly depends on the tidal regime of the region considered. The regions where macro-tidal regimes exist are very few around the world and should be treated separately in such computations since often results are very different there, as shown by our results. Another region where similar order of magnitude RMS misfits have been obtained is in the NW of Australia. Ray (2008) shows that there RMS misfit for M2 obtained between 160 TGs and solutions extracted from GOT4.7 and FES04 are 14.4 cm and 22.2 cm respectively. We obtained very similar results with these two models on the Patagonian shelf (Table 3).

If the RSS of the five tidal components is analyzed for each station separately (Figure 6) it is possible to observe several things that provide information about the regions where models encounter more difficulties. At Mar del Plata (MDP) global models obtain a better agreement compared to regional models. This can be due to a couple of factors: (i) The TG at MDP is better located compared to the other three TGs since it is not located inside a bay or an estuary, a fact that can represent an important limitation, especially to low-resolution models; (ii) T/P track 26 passes very close (4km) to the TG located at MDP, while no tracks pass closer than 50 km to the other three TG considered (T/P tracks and TG positions are plotted on Figure 1).

At Puerto Madryn SMARA presents the largest RSS misfit (Figure 6). This is due to the fact that the amplitude difference between the model and the TG for the M_2 constituent is l.2 m, probably due to both the location of the TG (inside a bay) and the resolution of the model. The same amplitude difference at Puerto Madryn is also noted in Etala (2009).

3.2 Continental shelf analysis: comparison to satellite data

Results from altimeters over the shelf are more encouraging than those obtained with the coastal TGs. Global models clearly show a better agreement than local models when compared with altimetry data over the shelf (Table 4, Figure 7). The best result considering all the crossovers over the shelf is obtained by TPXO_AO, with an RSS of 4.1 cm for the five constituents M_2, N_2, S_2, K_1 and O_1 (Table 4). This value is close to those obtained in other marginal seas (e.g. Matsumoto et al., 2000). The fact that global models get better results over the shelf compared to local models is not surprising considering that all the global models considered assimilate altimetry data or incorporate empirical mapping of the tidal constituent. However, the fact that significant differences exist confirm what we argued in Section 2.4, i.e. that error propagation can be specially important over large shelf areas as on the Patagonian shelf. Comparing RSS results obtained considering the northern and southern part of the shelf (Table 4, Figure 7), higher values are found in the southern part for all models but one. The high tidal amplitudes that are present in the southern part compared to the northern part are certainly the main factor responsible for the higher RSS misfits founds in the southern region. The unique model that presents a larger misfit in the northern region than in the southern region is the model by Palma. The difference presented by this model compared to the others is also reflected in the cotidal charts (not shown): Palma's model shows a southernmost location of the amphidromic point located offshore Mar del Plata.

Among the local models, it is worth noting that despite the low resolution (1/3 of degree), the SMARA model obtains the best result by a large margin (RSS is lower than 6.3 cm and 15.1 cm, compared to the Simionato and Palma models, respectively).

As expected, all the models get better results in the open ocean (Table 4) where waters are deeper than 300 m. There, RSS for TPXO_AO is 2.7 cm, a value which is very close to the standard 2 cm RMS value that is usually applied to the T/P, J-1 and J-2 data as a nominal resolution in deep waters.

4. CONCLUSIONS AND DISCUSSION

4.1 Contribution from other constituents

The analysis presented in this work has so far discussed the 5 tidal constituents representing the common set solved by the models considered i.e. M_2, N_2, S_2, K_1 and O_1 (Table 2). Depending on

the location considered, constituents not considered here might contribute significantly to the tidal regime. It has been shown that the overtide M_4 has an important contribution in the southern part of the shelf (e.g. Glorioso and Flather, 1997, Simionato et al, 2004). To test if the constituents Q_1, P_1, K_2 and the overtide M_4 provide an important contribution to our RSS misfit computations, we estimate the RMS misfit between the models that provide these components and the TGs along the coast. Results indicate that the RMS misfit for Q_1 and P_1 constituents is similar to K_1 and O_1 constituents. On the other hand, the RMS for K_2 constituents is greater than K_1 and O_1 (Table 3). M_4 RMS misfit is, depending on the model considered, as large as or higher than the RMS obtained with N_2 or S_2. Depending on the model, the RSS misfit increased in a range that goes from 1.07 cm to 3.35 cm after adding the Q_1, P_1, K_2 and M_4 constituents discussed (Table 3). These results suggest that the main source of discrepancy between the models and the TGs comes from the components M_2, N_2, S_2 and M_4.

At the crossovers points over the continental shelf we added the analysis of the RMS misfit between altimetry and models for the K_2 and M_4 components. We do not consider P_1 and Q_1 since the expected amplitudes (as indicated by the models that do estimate these components, not shown) are lower or very close to the 3.9 cm T/P and Jason1 level of accuracy (http://podaac.jpl.nasa.gov/DATA_CATALOG/jason1info.html) for most of the region considered. Results are presented in column 10 of Table 4. TPXO_AO obtained the lowest RSS (4.5 cm) and the lowest RMS misfit (0.6 cm) of Table 4 for the M_4 overtide. This result indicates the good performance of the TPXO_AO model to compute the M_4 overtide.

4.2 Regional versus Global modelling

RSS misfits between models and TGs show that close to the coast two of the regional models considered (Palma and Simionato) perform better than the rest of the models (Table 3). Over the shelf global models clearly perform better than regional models (Table 4). The best result obtained over the shelf by TPXO_AO is probably due to the higher spatial resolution. Both for regional and global models, the RMS obtained for M_2 is the highest among each model, and therefore is the one that contributes the most to the respective RSS. A similar result was found by Burrage et al., (2003) in the macro-tidal region of the Southern Great Barrier Reef Lagoon (NE Australia); they found better results with a regional model while offshore a global model showed sufficient accuracy.

4.3 General conclusions and observations

As stated in the introduction, AVISO is moving from using GOT00 to GOT47 to produce their global gridded interpolated SSH data. In light of the results obtained (Table 3 and Table 4), the advantages of using GOT47 in lieu of GOT00 are evident in the comparison with the TGs and north of 42ºS with the altimetry data. However, it is remarked that there are tide models that perform much better: TPXO_AO over the shelf and Palma along the coast obtain almost half the RSS obtained by GOT00 or GOT47. Spatial and temporal resolution of satellite altimetry is not optimal to retrieve complex tidal regimes (Benveniste and Vignudelli, 2009), such as the one existing over the Patagonian shelf. Considering that regional models perform better than global models close to the coast, it can be argued that assimilating satellite altimetry data constrains global models to less realistic solutions over the shelf. Independent data are necessary to objectively discern if global or regional models perform better over the shelf.

The fact that the RSS misfit obtained with the TGs is an order of magnitude higher than the RMS misfit obtained with the altimetry data may be due to different factors. Since altimetry data degrade their quality as they approach the coast (as discussed in the introduction) and TPXO_AO assimilate altimetry data, it is possible that better results can be obtained if altimetry data are not assimilated into the model when they are close to the coast. To estimate how close to the coast altimeter data are comparable to TG data Saraceno et al (2008b) correlate altimeter along track data with the time series of the TG located at Mar del Plata, which passes only 4 km away from the ascending pass # 26 of T/P, J-1 and J-2. (Saraceno et al., 2008b) found that the correlation decreases at distances shorter than 40 km from the coast. Similar comparisons between altimeter and TG data have found similar values in other regions of the world (e.g. Saraceno et al., 2008a; Bouffard et al., 2008; Benveniste and Vignudelli, 2009).

Ray et al., (2009) compared four of the global models analyzed here (FES04, GOT47, GOT00 and TPXO) in terms of their contribution to Gravity Recovery and Climate Experiment (GRACE) satellite-to-satellite tracking residuals at global scale. Their results (see their Figure 9) clearly show that the Patagonian shelf is one of the regions where the highest misfits occur, in agreement with the observation that our RSS misfits are among the highest compared to values obtained in other regions.

4.4 Geostrophic velocities and future work

Geostrophic velocities can be estimated from SSH. For along track estimations a relationship between the error (S) in height and the error in the cross-track velocity can be obtained by propagating the former through the geostrophic calculation, assuming that errors in height are uncorrelated (Strub et al., 1997):

$$S_v^{\,2} = 2S_H^{\,2}\left(\frac{\partial V}{\partial H}\right)^2 = 2S_H^{\,2}\left(\frac{g}{fL}\right)^2 \qquad (2)$$

where f is the Coriolis parameter, g the gravity, L the along-track distance used to filter the SSH data and the subscripts H and v refers to SSH and geostrophic velocity respectively. A good value for L is 62 km (see Strub et al., 1997, for a discussion). Considering L = 62 km and the best result obtained by the tide models in the Patagonian shelf, i.e. an RSS of 4.4 cm (Table 4) as a value for S_H, formula (2) indicates that the RMS of the altimeter geostrophic velocities will be 9.9 cm/s at 43ºS. Clearly, considering larger values for L decreases this value and thus a compromise between the spatial scales filtered out, and the velocity error that can be accepted, must be found. There may be specific instances when it is worth pushing the spatial resolution to smaller scales, but only if the signal is strong enough to stand out above the increased noise. Over the Patagonian shelf current meter measurements deployed at 43ºS indicated that non-tidal currents may be larger than 10 cm/s at the mid-shelf but not close to the coast (Balestrini et al., 1996; Rivas, 1997). Thus, it is expected that only far from the coast accurate geostrophic velocities can be estimated using correctly de-tided altimeter values. Closer to the coast, the amplitude of non-tidal currents is lower than what can be solved with the altimeter measurements (about 10 cm/s) corrected with the best tide model available.

In the above reasoning, only the tide model misfit has been considered as a source of error for the SSH. Over the SWA continental shelf, and especially on the southern part, the tide model misfit is likely to be the main source of error. However it should be stressed that other source of errors like the wet atmospheric correction may have large contributions as well (Benveniste and Vignudelli, 2009). Fortunately, it has been shown that errors decrease considerably when information from different satellites missions are combined to obtain gridded values (Pascual et al., 2006; Ducet et al., 2000).

Future swath satellite altimetry has been designed to resolve mesoscale features at every pass (e.g. (Fu et al., 2010) and thus data to be obtained will be extremely useful in coastal regions. In the meantime we plan to de-tide all the altimeter data available using TPXO_AO and interpolate them in space and time to obtain, at least, accurate seasonal fields of SSH and geostrophic velocities as estimated from satellite altimetry over the shelf. As per the discussion above, the analysis will not include the 40 km close to the coast. A local tide model with very high resolution that assimilates in-situ and satellite data should yield the precision needed to estimate geostrophic velocities at a higher resolution both close to the coast and over the Patagonian shelf.

AKNOWLEDGMENTS

Support for MS for this work was provided through grant BID 1728/OC-AR PICT 2006/94. Partial support for an earlier version of this work was also provided by project X176 of UBACYT 2008-2010. Partial support for EED, MEF and WHG was provided by project I014 UBACYT 2008-2010. Altimetry data used in this study were developed, validated, and distributed by the CTOH/LEGOS, France. Careful reviews by two anonymous reviewers resulted in a clearer and more concise paper.

REFERENCES

Acha, E. M., H. W. Mianzan, R. A. Guerrero, M. Favero, and J. Bava (2004), Marine fronts at the continental shelves of austral South America - Physical and ecological processes, *Journal of Marine Systems*, *44*, 83-105.

Andersen, O. B., P. L. Woodworth, and R. A. Flather (1995), Intercomparison of recent ocean tide models, *Journal of Geophysical Research*, *100*(C12).

Backhaus, J.O., 1983. A semi-implicit scheme for the shallow water equations for application to shelf sea modelling. Continental ShelfResearch 2 (4), 243e254.

Backhaus, J.O., 1985. A three dimensional model for simulation of shelf sea dynamics. Deutsche Hydrographische Zeitschirft 38 (H.4), 164e187.

Balestrini, C., A.L. Rivas, A.R. Piola, A.A. Bianchi y R.A. Guerrero (1996), Corrientes en la plataforma continental argentina (43°S), Departamento Oceanografía, Servicio de Hidrografía Naval Informe Técnico N°94, 35pp.

Benveniste, J., and S. Vignudelli (2009), Challenges in Coastal Satellite Radar Altimetry, *Eos Trans. AGU*, *90*(26), 225.

Bianchi, A. A., L. Bianucci, A. R. Piola, D. R. Pino, I. Schloss, A. Poisson, and C. F. Balestrini (2005), Vertical stratification and air-sea CO2 fluxes in the Patagonian shelf, *Journal of Geophysical Research C: Oceans*, *110*(7), 1-10.

Blumberg, A. F., and G. L. Mellor (1987), A description of a threedimensional coastal ocean circulation model, in Three-Dimensional Coastal Ocean Models, Coastal Estuarine Sci. Ser., vol. 2, edited by N. Heaps, pp. 1 –16, AGU, Washington D. C.

Bouffard, J., S. Vignudelli, P. Cipollini and Y. Menard (2008), *Geophysical Research Letters, 35*, doi:10.1029/2008GL033488.

Burrage, D. M., C. R. Steinberg, L. B. Mason, and L. Bode (2003), Tidal corrections for TOPEX altimetry in the Coral Sea and Great Barrier Reef Lagoon: Comparisons with long-term tide gauge records, *J. Geophys. Res.*, *108*(C7).

Cancet, M., F. Birol, L. Roblou, C. Langlais, K. Guihou, J. Bouffard, R. Dussurget, R. Morrow, and F. Lyard (2009), CTOH Regional Altimetry Products: Examples of Applications, in *Proceedings of OceanObs'09: Sustained Ocean Observations and Information for Society (Annex),* Venice, Italy, 21-25 September 2009, Hall, J., Harrison, D.E. & Stammer, D., Eds., ESA Publication WPP-306.

Cartwright, D. E., and R. D. Ray (1990), Oceanic tides from Geosat altimetry, *J. Geophys. Res.*, *95*, 3069-3090.

Castro, B. M., and L. B. Miranda (1998), Physical oceanography of the western Atlantic continental shelf located between 4N and 34S, in The Sea, vol. 11, edited by A. R. Robinson and K. H. Brink, pp. 209–251, John Wiley, Hoboken, N. J.

Chelton, D., and M. G. Schlax (2003), The accuracies of smoothed sea surface height fields constructed from tandem satellite altimeter datasets, *Journal of Atmospheric and Oceanic Technology*, *20*, 1276-1302.

Cherniawsky, J. Y., M. G. G. Foreman, W. R. Crawford, and B. D. Beckley (2004), Altimeter observations of sea-level variability off the west coast of North America, *International Journal of Remote Sensing*, *25*(7), 1303-1306.

D'Onofrio, E. E., M. M. E. Fiore, and S. I. Romero (1999), Return periods of extreme water levels estimated for some vulnerable areas of Buenos Aires, *Continental Shelf Research*, *19*(13), 1681-1693.

Desai, S. D., and J. M. Wahr (1994), Another ocean tide model derived from TOPEX/POSEIDON satellite altimetry, *Eos Trans. AGU*, *75*(44), Fall Meet. Suppl., F57.

Ducet, N., P. Y. L. Traon, and G. Reverdin (2000), Global high-resolution mapping of ocean circulation from TOPEX/Poseidon and ERS-1 and -2, *J. Geophys. Res.*, *105*(C8), 19477 - 19498, doi:10.1029/2000JC900063.

Eanes, R. J. and S. V. Bettadpur (1995), The CSR3.0 global ocean tide model, *Report*, Univ. of Tex. at Austin, Cent. for Space Res.

Egbert, G. D., and S. Y. Erofeeva (2002), Efficient inverse modeling of barotropic ocean tides, *Journal of Atmospheric and Oceanic Technology*, *19*(2), 183-204.

Etala, P. (2009), Dynamic issues in the SE South America storm surge modeling, *Natural Hazards*, *51*(1), 79-95.

Fiore, M. M. E., E. E. D'Onofrio, J. L. Pousa, E. J. Schnack, and G. R. Bértola (2009), Storm surges and coastal impacts at Mar del Plata, Argentina, *Continental Shelf Research*, *29*(14), 1643-1649.

Foreman, M. G. G., W. R. Crawford, J. Y. Cherniawsky, J. F. R. Gower, L. Cuypers, and V. A. Ballantyne (1998), Tidal correction of TOPEX/POSEIDON altimetry for seasonal sea surface elevation and current determination off the Pacific coast of Canada, *J. Geophys. Res.*, *103*(C12), 27,979-927,998.

Fu, L. L. (2009), Pattern and velocity of propagation of the global ocean eddy variability, *Journal of Geophysical Research*, *114*(C11017), 1-14.

Fu, L-L, D. Alsdorf, E. Rodriguez, R. Morrow, N. Mognard, J. Lambin, P. Vaze, and T. Lafon, (2010), The SWOT (Surface Water and Ocean Topography) Mission, in *Proceedings of OceanObs'09: Sustained Ocean Observations and Information for Society (Vol. 2),* Venice, Italy, 21-25 September 2009, Hall, J., Harrison D.E. & Stammer, D., Eds., ESA Publication WPP-306.

Genco, M. L., F. Lyard, and C. Le Provost (1994), The oceanic tides in the South Atlantic Ocean, Ann. Geophys., 12, 868–886.

Glorioso, P. D. (2000), Patagonian shelf 3D tide and surge model, *Journal of Marine Systems*, *24*(1-2), 141-151.

Glorioso, P. D., and R. A. Flather (1997), The Patagonian Shelf tides, *Progress in Oceanography*, *40*(1-4), 263-283.

Khanta, L. H. (1995), Barotropic tides in the global oceans from a nonlinear tidal model assimilating altimetric tides: 1. Model description and results, J. Geophys. Res., 100, 4653– 4672.

Le Provost, C., M. L. Genco, F. Lyard, P. Vincent, and P. Canceil (1994), Spectroscopy of the world ocean tides from a finite element hydrodynamic model, *J. Geophys. Res., 99*, 24777– 24797.

Le Provost, C., F. Lyard, J. M. Molines, M. L. Genco, and F. Rabilloud (1998), A hydrodynamic ocean tide model improved by assimilating a satellite altimeter-derived data set, *J. Geophys. Res.*, *103*, 5513-5529.

Le Traon, P. Y., and G. Dibarboure (2002), Velocity mapping capabilities of present and future altimeter missions: The role of high frequency signals, *J. Atmos. Oceanic Technol.*, *19,* (2077-2088).

Leeuwenburgh, O., and D. Stammer (2002), Uncertainties in altimetry-based velocity estimates, *Journal of Geophysical Research (Oceans)*, *107*(C10), 3175.

Lyard, F., F. Lefevre, T. Letellier, and O. Francis (2006), Modelling the global ocean tides: Modern insights from FES2004, *Ocean Dynamics*, *56*(5-6), 394-415.

Matsumoto, K., Takanezawa, T., Ooe, M. (2000), Ocean tide models developed by assimilating TOPEX/POSEIDON altimeter data into hydrodynamic model: A global model and a regional model around Japan, *J. Oceanogr.*, *56*, 567-581;

Palma, E. D., R. P. Matano, and A. R. Piola (2004), A numerical study of the Southwestern Atlantic Shelf circulation: Barotropic response to tidal and wind forcing, *Journal of Geophysical Research C: Oceans*, *109*(8).

Palma, E. D., R. P. Matano, and A. R. Piola (2008), A numerical study of the Southwestern Atlantic Shelf circulation: Stratified ocean response to local and offshore forcing, *Journal of Geophysical Research C: Oceans*, *113*(11).

Panella S., Michelato A., Perdicaro R., Magazzù G., Decembrini S. and Scarazzato P. (1991), A preliminary contribution to understanding the hydrological characteristics of the Strait of Magellan: Austral spring 1989. *Boll. Ocean. Teor. Appl., 9*, 107-126.

Parke, M. E. (1987), Applicability of sattelite altimetry data to tidal models, ASCE, Williamsburg, VA, USA.

Parke, M. E., R. H. Stewart, D. L. Farless, and D. E. Cartwright (1987), On the choice of orbits for an altimetric satellite to study ocean circulation and tides, *J. Geophys. Res.*, *92*(11,693-11,707).

Pascual, A., Y. Faugere, G. Larnicol, and P.-Y. Le Traon (2006), Improved description of the ocean mesoscale variability by combining four satellite altimeters, *Geophysical Research Letters*, *33*, 02611.

Pascual, A., M.-I. Pujol, G. Larnicol, P.-Y. Le Traon, and M.-H. Rio (2007), Mesoscale mapping capabilities of multisatellite altimeter missions: First results with real data in the Mediterranean Sea, *Journal of Marine Systems*, *65*, 190-211.

Piola, A. R., S. I. Romero, and U. Zajaczkovski (2008), Space-time variability of the Plata plume inferred from ocean color, *Continental Shelf Research*, *28*(13), 1556-1567.

Ray, R. D. (1999), A global ocean tide model from TOPEX/POSEIDON altimetry: GOT99.2, Rep. NASA/M-1999-209478*Rep.*, 58 pp, Goddard Space Flight Center, Greenbelt, Md.

Ray, R. D. (2008), Tide Corrections for Shallow-Water Altimetry. A quick overview, Coastal Altimetry Workshop, Pisa, Italy, Nov. 2008, *www.coastalt.eu/pisaworkshop08/pres/03-ray_coastal.pdf* .

Ray, R. D., S. B. Luthcke and J.-P. Boy (2009), Qualitative comparisons of global ocean tide models by analysis of intersatellite ranging data, *J. Geophys. Res.*, *114*, C09017.

Rivas, A. L. (1997), Current-meter observations in the Argentine Continental Shelf, *Continental Shelf Research*, *17*, 391-406.

Romero, S. I., A. R. Piola, M. Charo, and C. A. Eiras Garcia (2006), Chlorophyll-a variability off Patagonia based on SeaWiFS data, *Journal of Geophysical Research C: Oceans*, *111*(5).

Saraceno, M., P. T. Strub, and P. M. Kosro (2008a), Estimates of sea surface height and near-surface alongshore coastal currents from combinations of altimeters and tide gauges, *Journal of Geophysical Research C: Oceans*, *113*(11).

Saraceno, M., E. E. D'Onofrio, M. E. Fiore, and W. H. Grismeyer (2008b), On the Utilization of Satellite Sea Surface Height Over the Argentinean Continental Shelf, paper presented at Second Coastal Altimetry Workshop, Pisa, Italy.

Savcenko, R., and W. Bosch (2008), EOT08a—Empirical ocean tide model from multi-mission satellite altimetry, *DGFI Report No.81*, 37 pp.

Schrama, E. J. O., and R. D. Ray (1994), A preliminary tidal analysis of TOPEX/POSEIDON altimetry, *Journal of Geophysical Research*, 99(C12).

Schwiderski, E. W. (1978), Global Ocean Tides, Part I: A Detailed Hydrodynamical Interpolation Model, NSWC/DL TR-3866, Naval Surface Weapons Center, Silver Spring, Maryland. 26 pp.

Schwiderski, E. W. (1980), On Charting Global Ocean Tides, Reviews of Geophysics and Space Physics, 18, No 1, 243-268.

SHN (2008), Tablas de Marea, Buenos Aires, Argentina: Servicio Hidrografia Naval, *Ministerio de Defensa* Publicación H 610, 643 pp.

Shum, C. K., et al. (1997), Accuracy assessment of recent ocean tide models, *J. Geophys. Res., 102*, 25173– 25194.

Simionato, C. G., W. Dragani, M. Nuñez, and M. Engel (2004), A set of 3-D nested models for tidal propagation from the argentinean continental shelf to the Río de la Plata estuary - Part I. M2., *Journal of Coastal Research*, *20*(3), 893-912.

Smith, W. H. F., and D. T. Sandwell (1997), Global Sea Floor Topography from Satellite Altimetry and Ship Depth Soundings Science, *Science*, *277*, 1956-1962.

Strub, P. T., T. K. Chereskin, P. P. Niiler, C. James, and M. D. Levine (1997), Altimeter-derived variability of surface velocities in the California Current System 1. Evaluation of TOPEX altimeter velocity resolution, *Journal of Geophysical Research*, *102*, 12727-12748.

Volkov, D. L., G. Larnicol, and J. Dorandeu (2007), Improving the quality of satellite altimetry data over continental shelves, *J. Geophys. Res.*, *112*(C06020).

Zavialov, P., O. Moller, and E. Campos (2002), First direct measurements of currents on the continental shelf of southern Brazil, Cont. Shelf Res., 22, 1975– 1986.

TABLES

Table 1. Location of the coastal sea level gauges, type of device and length of the corresponding time series. Indexes in parenthesis in the first column refer to locations in Figure 1.

Table 2. Main properties of tidal models used.

Table 3. RMS misfit between models and all the TGs for M2 (2nd column) and TGs 12, 17, 20 and 23 for the nine tidal constituents appearing (columns 3-11). The Root Sum Square (RSS) of the first five (nine) constituents indicated in columns 3-7 (3-11) are indicated in column 12 (13). Numbers in parenthesis in columns 2 and 12 indicate the three lowest values in the column. All values are in cm.

Table 4. RMS misfit between models and altimeter data for the five main tidal components at the altimeter crossover locations. The table has separate entries for the values over the shelf (less than 300 m depth) and offshore (more than 300m depth). The Root Sum Square (RSS) of the first five and seven components is indicated for all the continental shelf (columns 9-10), and for the first five constituents south and north of 42ºS (respectively columns 11-12) and offshore (last column). Numbers in parenthesis in column 9 indicate the three lowest values in the column. All values in the table are in cm.

FIGURES

Figure 1. Position of the Tide Gauges (magenta dots) and of the crossovers (circles) considered for the comparison between tide models and observed amplitudes and phases. Location and name of the TG stations are indicated in Table 1. Background: bathymetry (Smith and Sandwell, 1997); diagonal lines correspond to the ascending and descending paths of the T/P and J-1 and J-2 missions; the eastern border of the shelf is represented by the 300m isobath (black contour).

Figure 2: amplitude (meters, left panel) and phase (degrees, right panel) for the M2 constituent as obtained with the TPXO_AO tide model.

Figure 3: amplitude (m) of constituents obtained by harmonic analysis (SHN, 2008) from the four longest time series obtained by TGs along the Patagonian shelf. Amplitude at Loyola for M2 is 3.7m.

Figure 4. Comparison of the RMS misfit obtained for M2 between each model and the two coastal tide gauge data sets.

Figure 5. Comparison of the RMS misfit obtained for each model and for each component considering coastal tide gauges 12, 17, 20 and 23 (dataset 2).

Figure 6. Comparison of the Root Sum Square (RSS) of the 5-constituent misfit obtained for each model and each station with dataset 2.

Figure 7: Comparison of the Root Sum Square (RSS) of the misfit obtained for each model and different subsets of altimetry data of the crossovers locations indicated in Figure 1.

Table 1. Location of the coastal sea level gauges, type of device and length of the corresponding time series. Indexes in parenthesis in the first column refer to locations in Figure 1.

Station (index)	Lat. (ºS)	Lon. (ºW)	Type of Device	N. of days
Martín Garcia (2)	-34.183	-58.250	Floater	2920
Colonia (3)	-34.467	-57.850	Floater	730
Buenos Aires (4)	-34.567	-58.383	Floater	14965
La Plata (5)	-34.833	-57.883	Floater	365
Montevideo (6)	-34.917	-56.217	Floater	1460
Punta del Este (7)	-34.903	-54.950	Floater	365
Torre Oyarvide (8)	-35.100	-57.133	Floater	4745
Par Uno (9)	-35.167	-56.317	Pres Sensor	330
San Clemente (10)	-36.350	-56.715	Floater	730
Pinamar (11)	-37.117	-56.850	Floater	1460
Mar del Plata (12)	-38.033	-57.517	NGWLMS	4748
Pto. Belgrano (13)	-38.883	-62.100	Floater	301
San Blas (14)	-40.550	-62.233	Tide Pole	38
San Antonio E (15)	-40.800	-64.867	Tide Pole	40
Punta Colorada (16)	-41.767	-65.000	Floater	271
Puerto Madryn (17)	-42.767	-65.033	Floater	13505
Santa Elena (18)	-44.517	-65.367	Tide Pole	31
Comdoro Rivadavia (19)	-45.867	-67.483	Floater	1825
Pto. Deseado (20)	-47.750	-65.917	Floater	3700
San Julian (21)	-49.250	-67.667	Tide Pole	45
Punta Quilla (22)	-50.117	-68.417	NGWLMS	180
Punta Loyola (23)	-51.606	-69.017	Tide Pole	365
Punta Vírgenes (24)	-52.394	-68.427	Tide Pole	38
San Sebastian (25)	-53.167	-68.500	Tide Pole	61
Río Grande (26)	-53.783	-67.650	Floater	180
Bahia Thetis (27)	-54.633	-65.250	Tide Pole	139

Table 2. Main properties of tidal models used

	Incorporated tidal information	Coverage	Resolution (x, y) deg	Constituents resolved	Reference
Simionato	none	SWA	1/3, 1/4	M_2 S_2 N_2 K_1 O_1 K_2 P_1 Q_1 M_4	(Simionato et al., 2004)
Palma	none	SWA	1/10, 1/10	M_2 S_2 N_2 K_1 O_1	(Palma et al., 2004)
SMARA	none	SWA	1/3, 1/3	M_2 S_2 N_2 K_1 O_1	(Etala, 2009b)
FES04	Assimilated TG+altimetry	Global	1/8, 1/8	M_2 S_2 N_2 K_1 O_1 K_2 P_1 Q_1 M_4 $2N_2$ Mf Mm Msqm Mtm	(Lyard et al., 2006)
GOT4.7	empirical mapping of the tidal constituent	Global	1/2, 1/2	M_2 S_2 N_2 K_1 O_1 K_2 P_1 Q_1 M_4 S_1	(Ray, 1999)
GOT00	empirical mapping of the tidal constituent	Global	1/2, 1/2	M_2 S_2 N_2 K_1 O_1 K_2 P1 Q_1 Mf	(Ray, 1999)
TPXO_AO	Assimilated TG+altimetry	Atlantic	1/12, 1/12	M_2 S_2 N_2 K_1 O_1 K_2 P_1 Q_1 M_4 MS_4 MN_4	(Egbert and Erofeeva, 2002)
EOT08a	empirical mapping of the tidal constituent	global	1/8, 1/8	M_2 S_2 N_2 K_1 O_1 K_2 P_1 Q_1 M_4 $2N_2$	(Savcenko and Bosch, 2008)

Table 3. RMS misfit between models and all the TGs for M_2 (2nd column) and TGs 12, 17, 20 and 23 for the nine tidal constituents appearing (columns 3-11). The Root Sum Square (RSS) of the first five (nine) constituents indicated in columns 3-7 (3-11) are indicated in column 12 (13). Numbers in parenthesis in columns 2 and 12 indicate the three lowest values in the column. All values are in cm.

	All TGs	Only TGs 12, 17, 20 and 23										
	M_2	M_2	N_2	S_2	K_1	O_1	Q_1	P_1	K_2	M_4	RSS 5	RSS 9
Palma	66.79	13.85	7.23	7.00	4.36	4.25					18.17 (1)	
Simionato	34.09	14.07	9.28	6.55	4.11	5.12	1.09	2.46	8.46	7.82	19.24 (2)	22.59
SMARA	34.44	45.94	12.30	16.53	4.90	4.76					50.81	
TPXO_AO	19.28 (3)	24.77	7.95	12.99	2.09	1.74	0.98	2.28	3.39	6.59	29.20	30.23
EOT08a	18.03 (1)	23.42	7.12	8.99	1.33	1.70	1.52	2.33	2.10	6.81	26.16	27.26
FES04	19.16 (2)	21.98	6.07	8.72	1.22	1.89	0.93	2.22	5.58	7.94	24.52 (3)	26.48
GOT4.7	20.24	28.60	7.84	10.53	1.55	2.30	0.85	1.98	2.97	7.55	31.59	32.69
GOT00	25.98	31.61	8.46	11.18	3.00	2.42	1.60	2.05	2.92		34.79	

Table 4. RMS misfit between models and altimeter data for the seven main tidal components at the altimeter crossover locations. The table has separate entries for the values over the shelf (less than 300 m depth) and offshore (more than 300m depth). The Root Sum Square (RSS) of the first five and seven components is indicated for all the continental shelf (columns 9-10), and for the first five constituents south and north of 42ºS (respectively columns 11-12) and offshore (last column). Numbers in parenthesis in column 9 indicate the three lowest values in the column. All values in the table are in cm.

	<300m											>300m
	Over the shelf									South of 42ºS	North of 42ºS	Offshore
	M_2	N_2	S_2	K_1	O_1	K_2	M_4	RSS 5	RSS 7	RSS 5	RSS 5	RSS 5
Palma	24.16	7.29	6.89	5.31	2.34	-	-	26.80	-	24.57	32.52	16.52
Simionato	16.08	2.53	8.97	2.30	3.06	3.87	2.63	18.98	19.54	20.24	14.04	4.29
SMARA	9.52	3.50	3.94	3.58	2.43	-	-	11.71	-	12.58	9.83	9.06
TPXO_AO	2.39	0.87	2.01	1.93	1.67	1.62	0.61	4.12 (1)	4.47	4.14	3.80	2.35
EOT08a	3.87	0.93	1.79	2.17	1.52	1.51	0.95	5.11 (2)	5.41	5.59	3.42	2.79
FES04	5.99	1.76	2.56	2.70	1.78	2.72	3.11	7.48	8.55	7.90	5.48	2.71
GOT4.7	5.95	1.55	2.46	2.17	1.78	1.66	1.25	7.20 (3)	7.49	7.38	5.78	2.49
GOT00	6.29	1.96	2.65	1.92	1.79	-	-	7.57	-	7.45	7.40	2.49

Figure 1

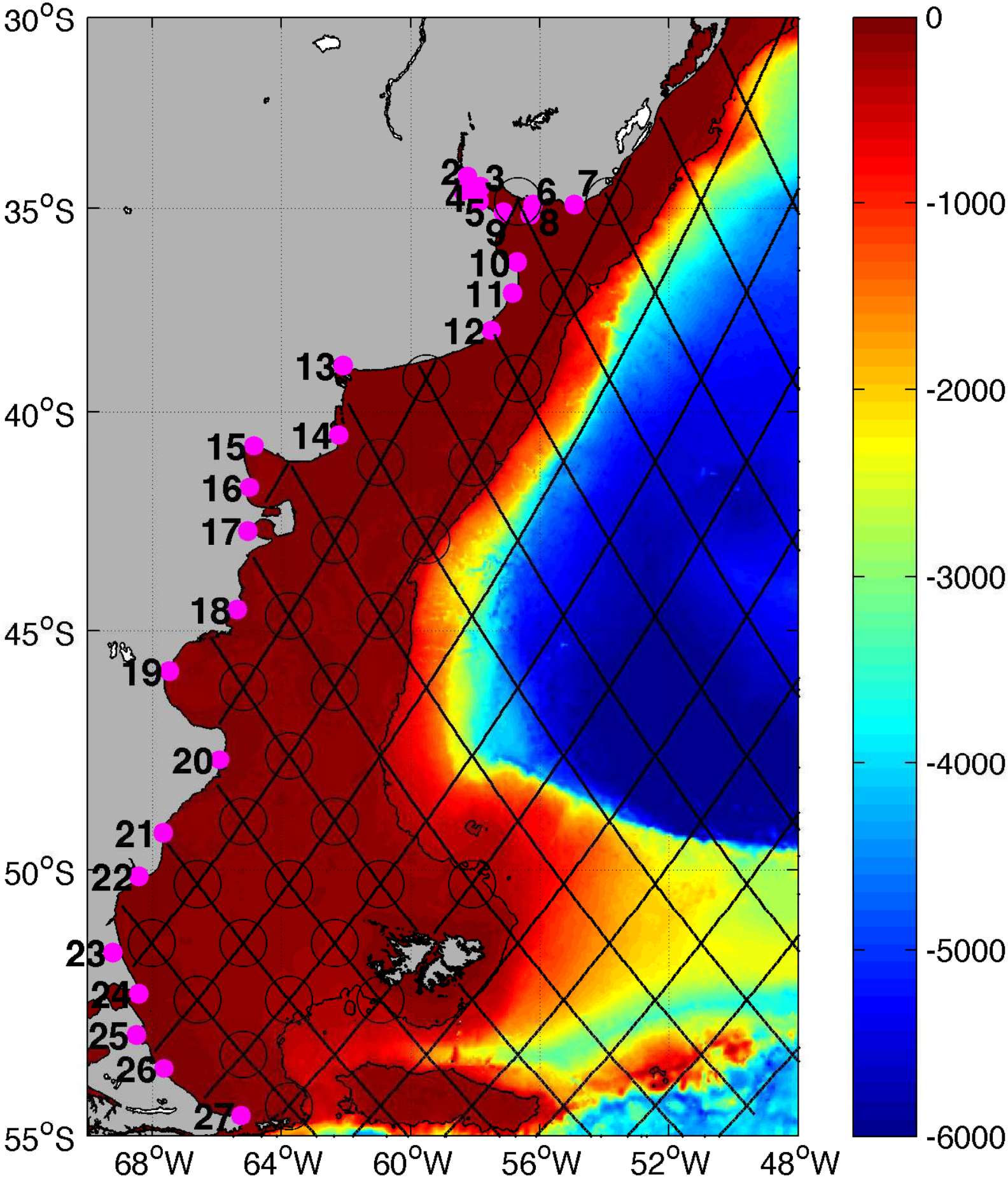

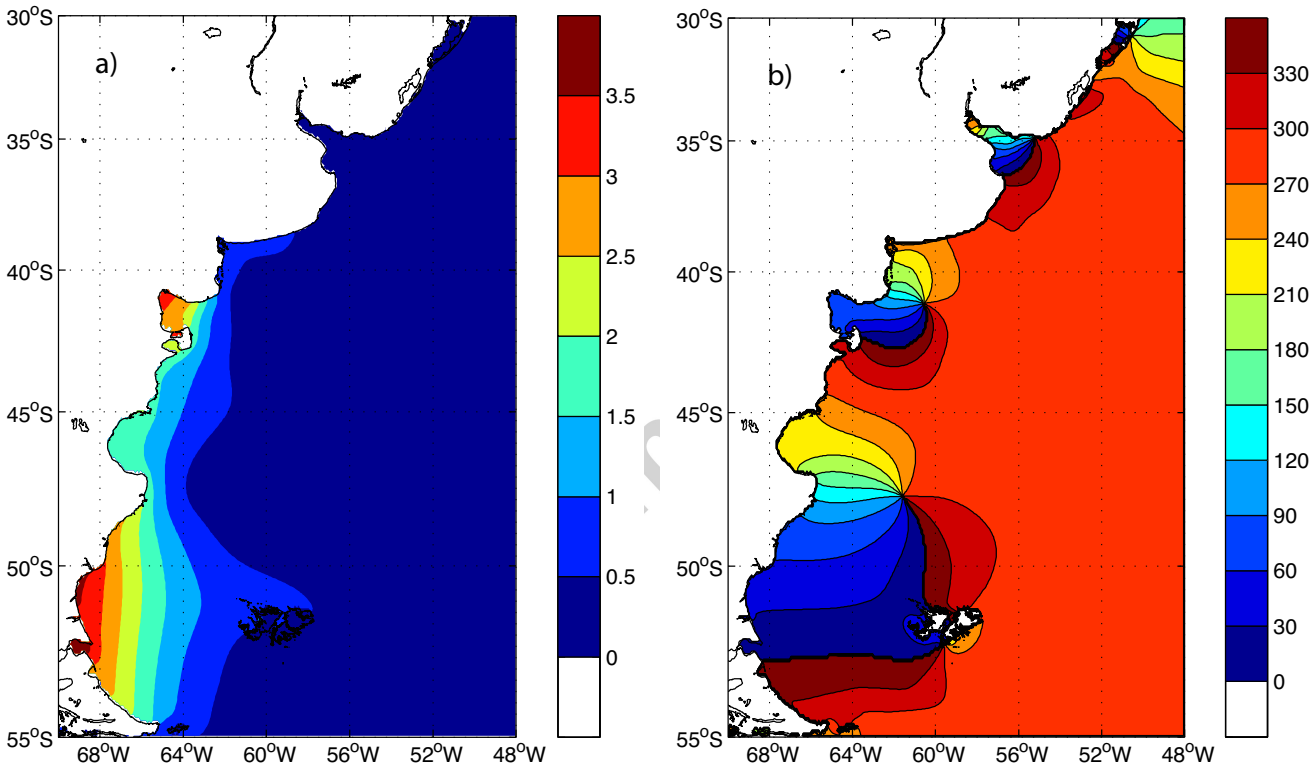

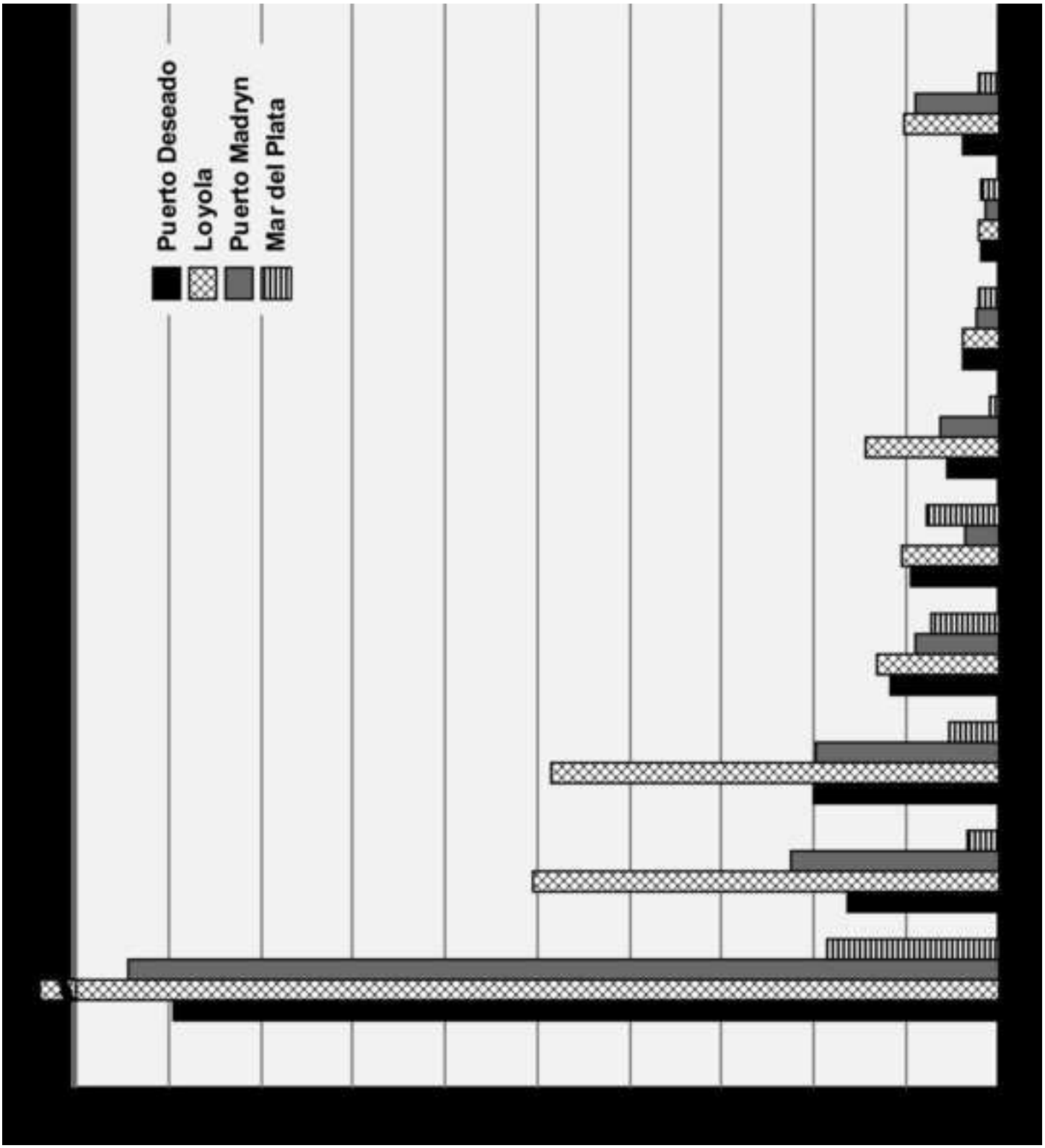

Figure 3

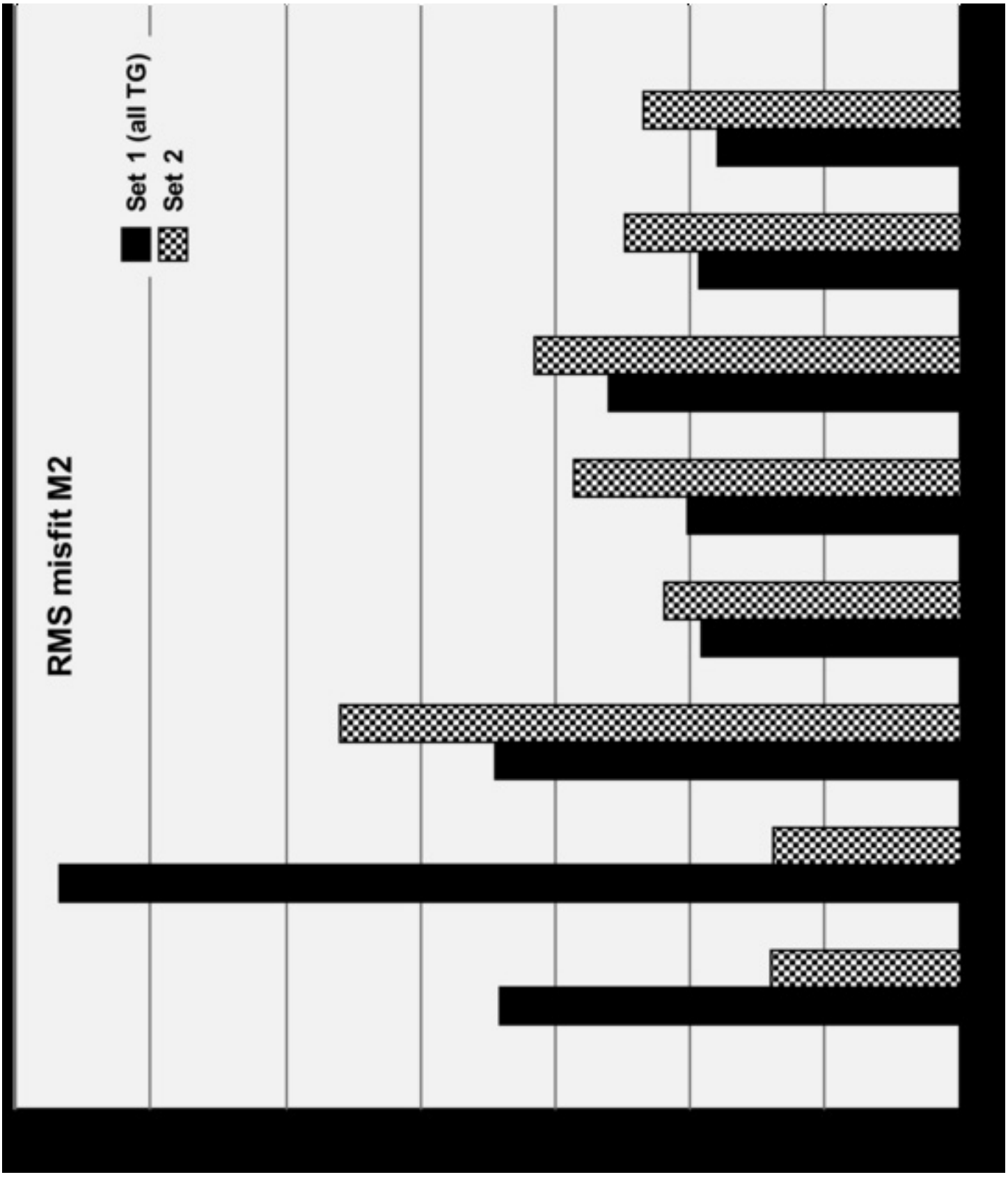

Figure 4

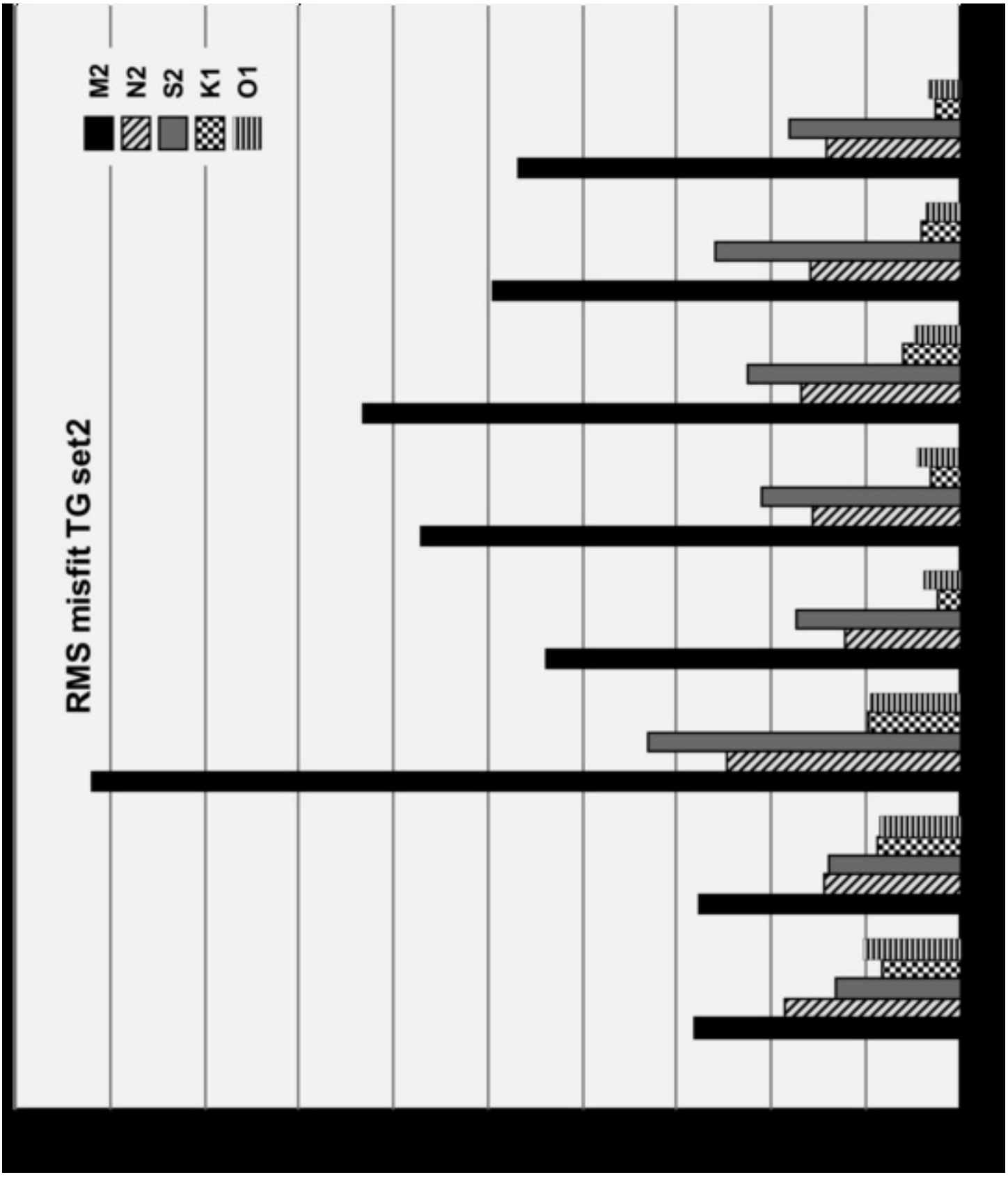

Figure 5

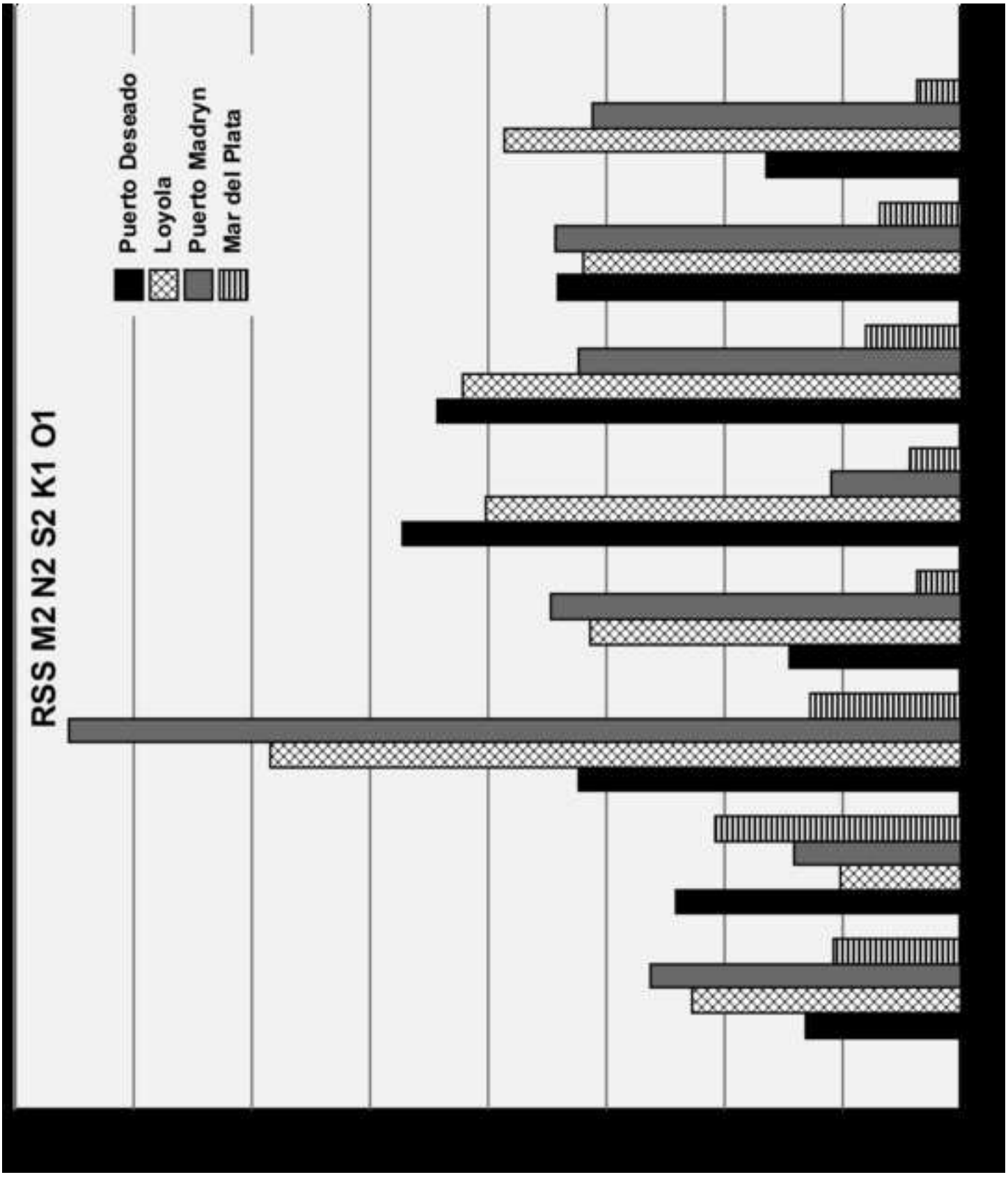
Puerto Deseado
Loyola
Puerto Madryn
Mar del Plata
RSS M2 N2 S2 K1 O1

Figure 6

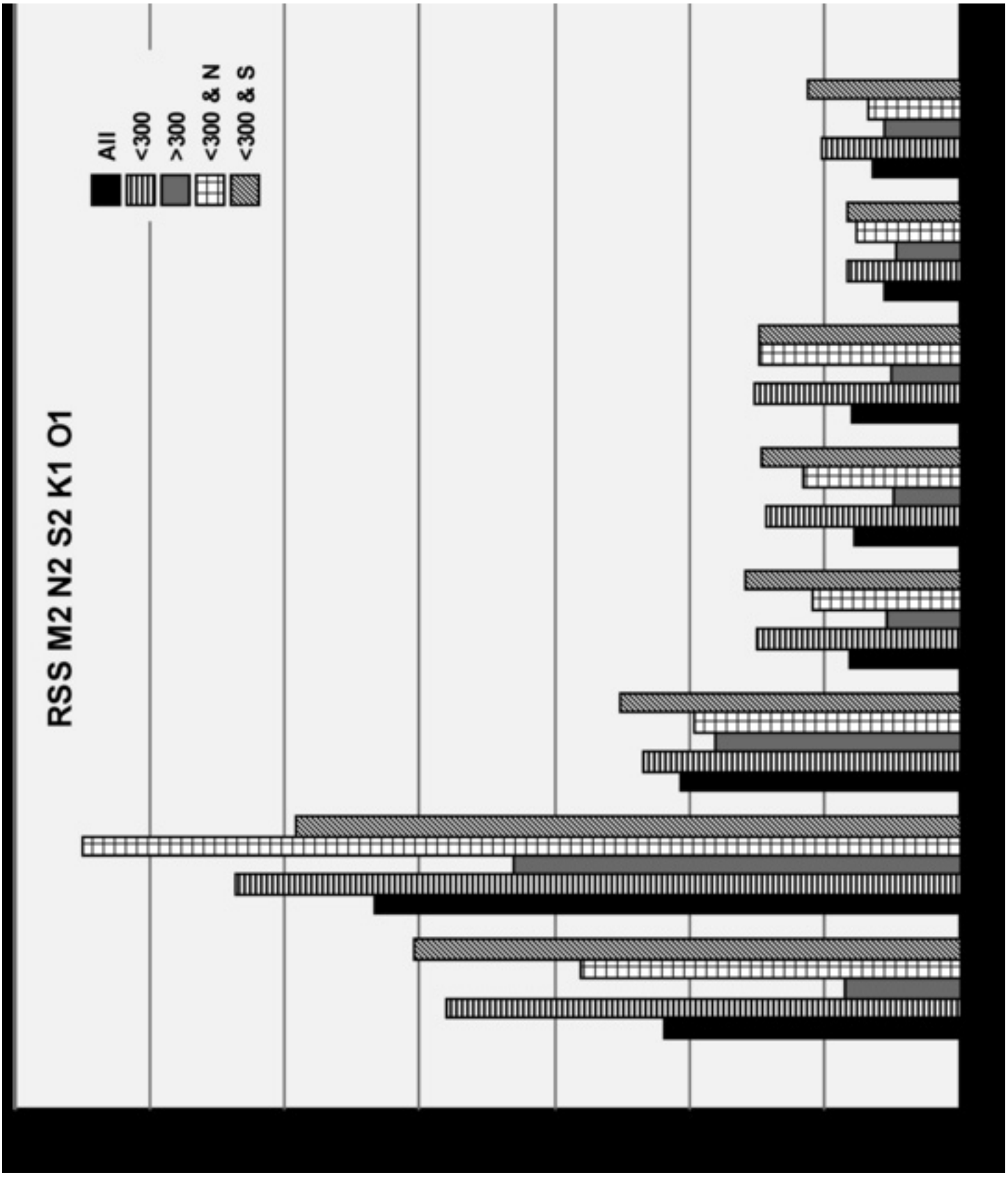

Figure 7